ARTICLE

Check for updates

Substantial increase in future fluvial flood risk projected in China's major urban agglomerations

Ruijie Jiang[1], Hui Lu [1,2✉], Kun Yang [1], Deliang Chen [3], Jiayue Zhou[1], Dai Yamazaki[4], Ming Pan[5,6], Wenyu Li[1], Nan Xu[1], Yuan Yang[5], Dabo Guan [1,7] & Fuqiang Tian [8]

Urban land will face high fluvial flood risk against the background of climate change and urban expansion. The effect of urban spatial expansion, instead of densification of assets within existing urban cells, on flood risk has rarely been reported. Here, we project the future flood risk of seven urban agglomerations in China, home to over 750 million people. The inundated urban land areas in the future are projected to be 4 to 19 times that at present. Without considering the urban spatial expansion, the inundated urban land areas will be underestimated by 10-50%. Urban land is more likely to be inundated than non-urban land, and the newly-developed urban land will be inundated more easily than the historical urban land. The results demonstrate the urgency of integrating climate change mitigation, reasonable urban land expansion, and increased flood protection levels to minimize the flood risk in urban land.

[1] Ministry of Education Key Laboratory for Earth System Modeling, Department of Earth System Science, Tsinghua University, Beijing, China. [2] Tsinghua University (Department of Earth System Science)- Xi'an Institute of Surveying and Mapping Joint Research Center for Next-Generation Smart Mapping, Beijing, China. [3] Regional Climate Group, Department of Earth Sciences, University of Gothenburg, Gothenburg, Sweden. [4] Institute of Industrial Science, The University of Tokyo, Tokyo, Japan. [5] Center for Western Weather and Water Extremes, Scripps Institution of Oceanography, University of California San Diego, La Jolla, California, USA. [6] Department of Civil and Environmental Engineering, Princeton University, Princeton, NJ, USA. [7] The Bartlett School of Sustainable Construction, University College London, London, UK. [8] Department of Hydraulic Engineering, State Key Laboratory of Hydroscience and Engineering, Tsinghua University, Beijing, China. ✉email: luhui@tsinghua.edu.cn

Floods are one of the most destructive natural disasters. In the past few decades, floods have caused annual losses on the order of tens of billions of dollars and thousands of casualties[1,2]. Ongoing global warming is increasing the water vapor capacity of the atmosphere, and thus the water cycle is accelerating[3,4], leading to an increase in the frequency and intensity of extreme hydrological events such as floods[5,6].

Currently, projections of future flood hazard and risk are mainly based on hydrological models driven by outputs from the Coupled Model Intercomparison Project 5 (CMIP5)[7–10], although the latest climate projection outputs have been produced by CMIP6[11]. China is greatly affected by floods; over the past 30 years, flood losses in China have accounted for about 10% of the global total[12]. Compared with CMIP5 outputs, CMIP6 outputs have improved the simulation of precipitation indices[13,14]. Hirabayashi et al. (2021) have projected the global population exposed to floods based on the CMIP6 outputs[15]. However, to the best of our knowledge, there have not been studies using bias-corrected CMIP6 outputs to project flood hazard in China.

In addition, socio-economic development has led to increased flood exposure[16–19]. Developing countries and emerging economies such as China are undergoing rapid urbanization. From 1992 to 2015, urban land area in floodplains increased by 542.21% in China, leading to high flood exposure[20]. For example, Zhengzhou, the core city of the Central Plains urban agglomeration in China, suffered a serious flood in July 2021, causing nearly 300 deaths[21].

Recent studies have evaluated flood risk by considering urban growth[22,23], and have found that the flood risk will increase due to the urban expansion. However, this research did not consider climate change. Winsemius et al.[24] have considered climate change, while they only considered the future densification of assets within historically existing urban cells (i.e., increasing population and economic activity in existing urban areas), and the increase in urban land extent is not considered. Therefore, the relative importance of climate change and urban expansion on flood risk remains unclear. Muis et al.[25] have considered both climate change and urban land expansion in the future. Their study period is from 2010 to 2049. However, the growth rate of urban land demand may slow down after 2050[26], and thus the relative importance of climate change and urban expansion to flood risk may vary across different periods. Besides, the urban land expansion data in Muis et al.[25] is not developed under the shared socioeconomic pathway (SSP) framework, while SSPs describe alternative evolutions of future society and can be better combined with climate simulations from CMIP6. Moreover, the effect of spatial pattern of urban land expansion on flood risk is rarely explored. Chen et al.[26] developed the global 1-km resolution maps of future urban land expansion under the SSP framework from 2020 to 2100, and flood maps can now be generated at 500 m resolution or even higher[27–29]. Therefore, the latest high-resolution urban expansion data are more suitable for combining with flood maps to explore the effect of urban land expansion on flood risk.

This study uses data from five contributions to the latest phase 3b of the Inter-Sectoral Impact Model Intercomparison Project (ISIMIP3b), which is bias-corrected from the CMIP6 outputs, to force the hydrological model Variable Infiltration Capacity (VIC) and generate daily runoff (See Methods section "Forcing data"). Then, the runoff is routed by the hydrodynamic model CaMa-Flood, to generate daily river discharge and flood extent under different warming levels (1.5°C, 2.0°C, 2.5°C and 3.0°C) and socio-economic scenarios (SSP1-2.6, SSP3-7.0, and SSP5-8.5). The inundation maps generated by CaMa-Flood are overlain with the latest urban land expansion data to generate inundated urban land areas. The inundated urban land areas were then used as an indicator to measure flood risk, and flood risk refers to the inundated urban land areas hereinafter. Throughout, unless specified differently, the results of the inundated urban land areas in this study refer to the ensemble median results based on the five global climate models (GCMs).

To make our study more representative, we focus on the urban agglomerations of (a) Beijing-Tianjin-Hebei (BTH), (b) Central Plains (CP), (c) Central Shanxi Plain (CSP), (d) Yangtze River Delta (YRD), (e) Triangle of Central China (TCC), (f) Chengdu-Chongqing (CC), (g) Pearl River Delta (PRD) and (h) the sum of these urban agglomerations. The seven urban agglomerations are located in the main floodplains of China, and have suffered severe flood losses during historical periods. Besides, these seven urban agglomerations account for 54% of China's population and 67% of its GDP (Supplementary Table 1). Therefore, the seven urban agglomerations may face high flood risk in the future. Furthermore, the urban land of selected urban agglomerations has different expansion patterns. Using these case studies, we can better explore the impact of urban land expansion on flood risk.

We find that the flood risk of these seven urban agglomerations will increase against the background of climate change and urban land expansion. The edge expansion pattern of urban land, increased extreme precipitation and low-level protection levels will put the future newly-developed urban land in danger.

Results

Future flood risk. With warming levels of 1.5 °C, 2 °C, 2.5 °C and 3 °C, the 30-year average annual inundated urban land areas of the seven urban agglomerations are projected to face respective increases of 4.7 to 8.3, 4.5 to 9.7, 10.8 to 12.8, and 15.5 to 19.0 times those of the historical period across different scenarios (Supplementary Table 4). These increases equate to areas of 110–190, 100–220, 250–290, and 350–430 square kilometers.

Considering the urban agglomerations individually (Fig. 1a), it is apparent that the inundated urban land areas of the PRD, CC, and TCC urban agglomerations will face the largest increases (Supplementary Table 4), indicating southern China will face great flood control pressure. The 30-year average annual inundated urban land areas in the YRD urban agglomeration are also very large, due to the large inundated areas in the historical period. It is also clear from Fig. 1a (e.g., in the YRD urban agglomeration) that the inundated urban land areas do not always increase continuously with a gradually warming climate. There are also differences between different scenarios: because the climate change is most severe under SSP5-8.5, the flood risk is also the most extreme in most of the cases under that scenario.

The above results show the projected inundated urban land areas and their relative changes, here we further investigate changes in the inundated proportion of urban land. As shown in Fig. 2, the 30-year average annual inundated proportion of urban land of the seven urban agglomerations in the historical period is equal to 0.04%. Considering the urban agglomerations individually, we note that the YRD, BTH, and CP urban agglomerations are located in large river basins, with flat terrain (Supplementary Fig. 1); consequently, these agglomerations have the highest 30-year average annual inundated proportion of urban land.

The inundated proportion of urban land shows a pronounced rise against the background of global warming and urban land expansion. With warming levels of 1.5 °C, 2 °C, 2.5 °C and 3 °C, the 30-year average annual inundated proportion of urban land will reach 0.20% to 0.32%, 0.20% to 0.36%, 0.42% to 0.44%, and 0.59% to 0.63%, respectively, when the different scenarios are considered. These are increases of 5 to 8, 5 to 9, 10 to 11, and 15 to 16 times those of the historical period. In terms of proportions, the most serious flood risk is projected in the PRD urban
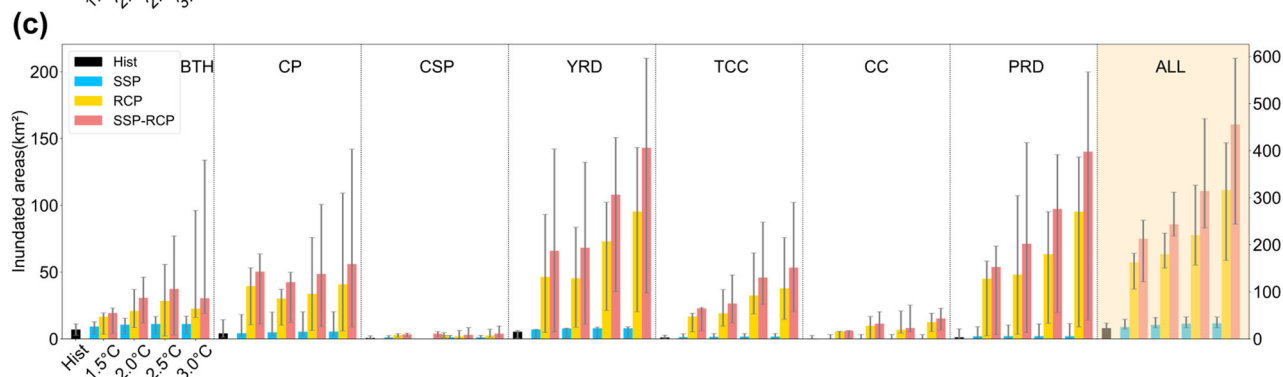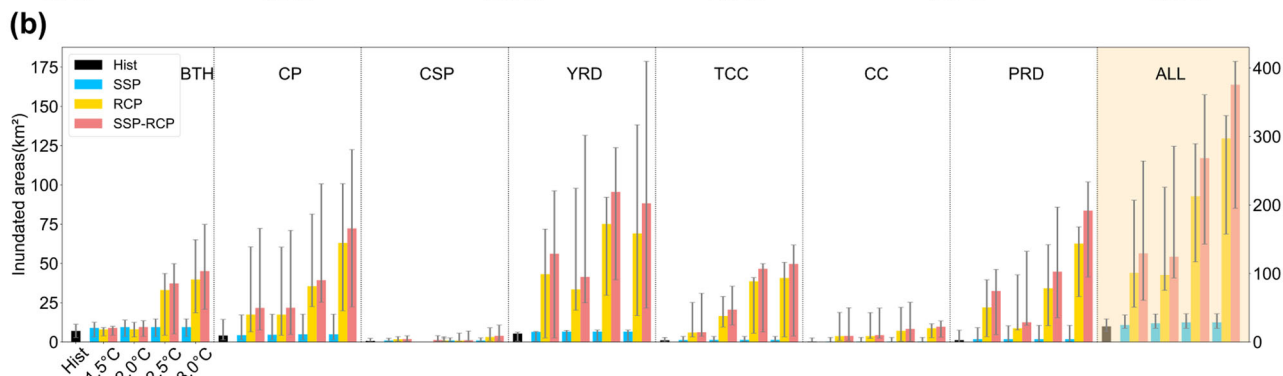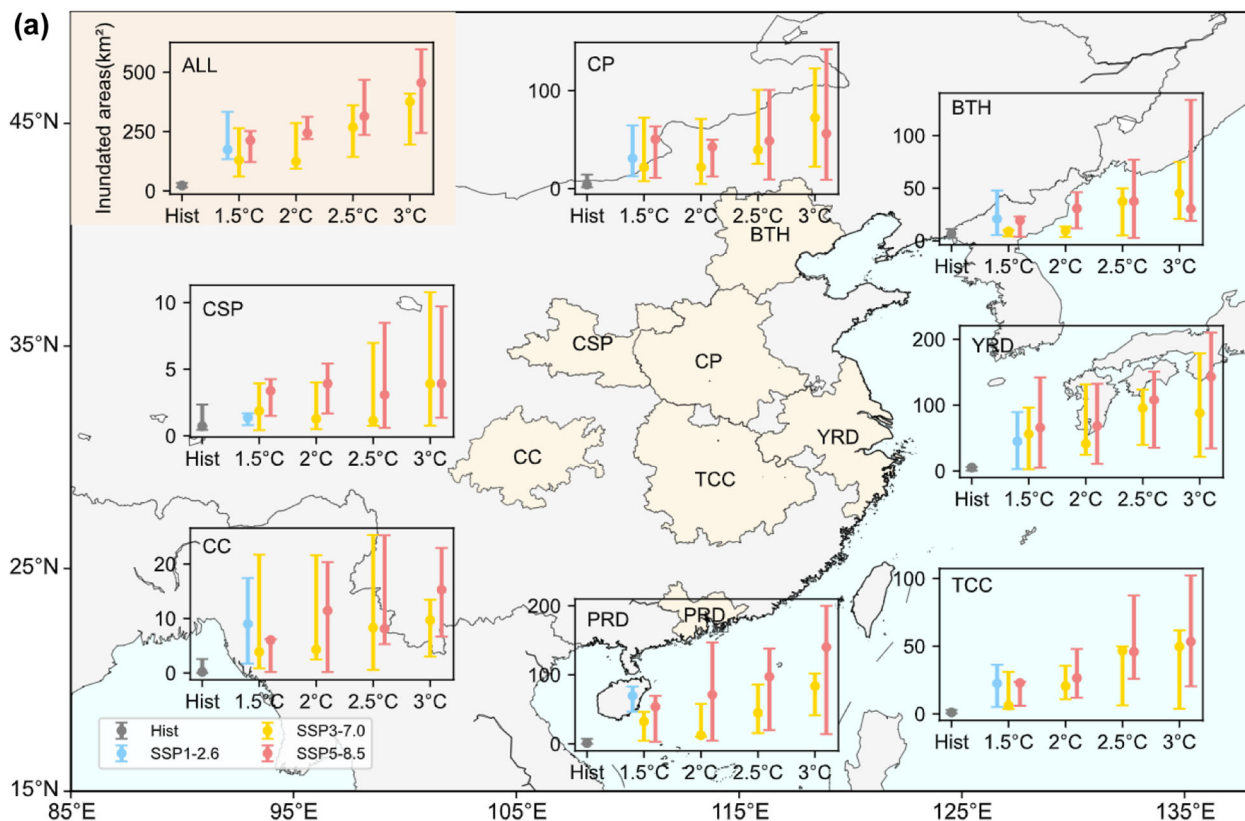
Fig. 1 The projected inundated urban land areas of the seven urban agglomerations. a 30-year average annual inundated urban land areas for the historical period (Hist) and future warming levels under different scenarios. The historical period, SSP1-2.6, SSP3-7.0, and SSP5-8.5 scenarios are represented by black, blue, yellow, and red lines, respectively. The circles are the ensemble median projections, with the spread indicated by the ensemble minimum and maximum. **b** 30-year average annual inundated urban land areas of each urban agglomeration under different assumptions for SSP3-7.0. RCP means only climate change is considered, SSP means only urban land expansion is considered, and SSP-RCP means both climate change and urban expansion are considered. Bars are the ensemble median, with the spread indicated by the ensemble minimum and maximum. Histograms within the shaded background refer to the right-hand y-axis scale. **c** The same as (**b**), but under SSP5-8.5.
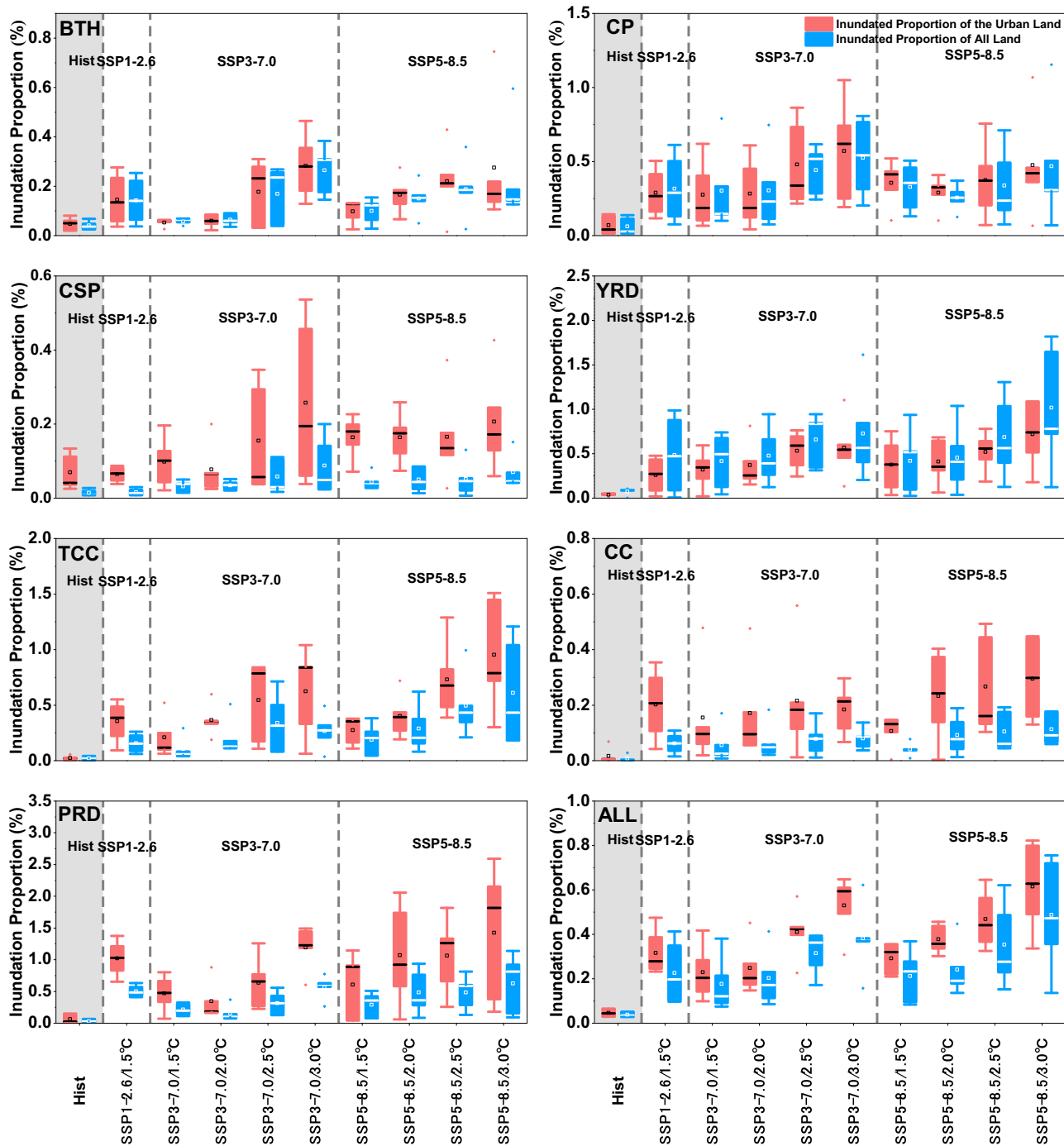
Fig. 2 The 30-year average annual inundated proportion of urban land (red) and total land (blue) of each urban agglomeration for the historical period (Hist) and different warming levels under each scenario. From top to bottom, the box-plot lines represent the maximum, 75% quantile, median, 25% quantile, and minimum. The dots represent the mean value.

agglomeration, where the annual inundated proportion of urban land is expected to rise to over 1% under all the scenarios.

Figure 2 also shows the inundated proportion of the total land areas in the urban agglomerations. It can be seen that, with the exception of the YRD urban agglomeration, the inundated proportion of urban land is greater than the inundated proportion of the total land areas and will increase by over 20%, which means that compared to non-urban land, urban land is more likely to be inundated. This is consistent with expectations and general knowledge, as we can see that most of the urban land is located along rivers (Supplementary Fig. 1).

Contributions of climate change and urban land expansion. The inundated urban land areas of the seven urban agglomerations will face tenfold increases (Fig. 1a), while we can see that the urban land areas will face 20–40% increases (Supplementary Fig. 2). Evidently, the growth rate of flood risk in urban land outpaces the growth rate of urban land, highlighting climate change may play a very important role in the strong rise in flood risk. To further explore the contributions of climate change and urban land expansion to the changes in projected inundated urban land areas in the future, we carried out a quantitative analysis (See Methods section "Calculation of flood risk").
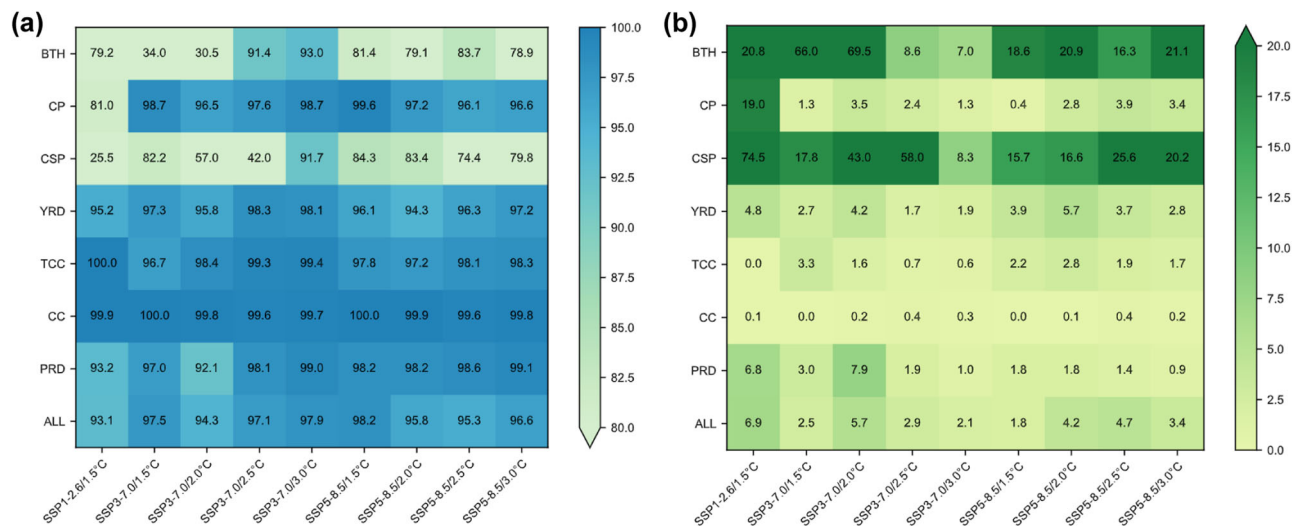
Fig. 3 Contributions of climate change and urban land expansion to the projected changes in inundated urban land areas (%). a Contributions of climate change. **b** Contributions of urban land expansion. Note that the contribution of climate change = 100% - contribution of urban expansion.

As shown in Fig. 3, climate change is the main driver. The contribution of climate change is larger than 50% in most cases, which may be partly explained by a substantial increase in extreme precipitation (Supplementary Figs. 3–5). The contribution of climate change is nearly 100% in southern China, while in northern China (e.g., BTH and CSP urban agglomerations), the urban expansion also plays an important role at some warming levels. This difference is related to many factors, such as the severity of climate change, the rate of urban land expansion, and the topography of the river network[30]. Supplementary Figures 6–8 show that the frequency of the 100-year floods corresponding to the historical period is expected to increase (i.e., the return period decreases) across most areas in China, while this change is not so notable in northern China (Supplementary Table 9). This may be one of the reasons why urban land expansion plays a relatively important role in the rise of inundated urban land areas in northern urban agglomerations. The other reason will be discussed in the following section "Effect of urban land expansion on flood risk". It is also apparent that the contribution of urban land expansion gradually decreases as the warming level reaches 2 °C, which is because the urban land stops expanding after 2040–2050 (Supplementary Fig. 2), while climate change becomes increasingly severe.

Effect of urban land expansion on flood risk. As the impact of climate change on flood risk has been deeply explored[7,31–33], here we further explore the impact of urban land expansion on flood risk. As shown in Fig. 1b, c, for both the SSP3-7.0 and SSP5-8.5 scenarios, when considering both climate change and urban land expansion, flood risk will be 10–50% higher than when climate change alone is considered. We next discuss the differences between the projected inundated urban land areas when (i) only considering climate change, and (ii) considering both climate change and urban land expansion.

Firstly, it can be seen from Supplementary Fig. 12 that the inundated newly-developed urban land areas are related to the total area of newly-developed urban land. The newly-developed urban land areas are the largest in the YRD urban agglomeration, and consequently, the inundated newly-developed urban land areas are also the largest in the YRD urban agglomeration. The CSP urban agglomeration represents the opposite case.

It is not only the total area of newly-developed urban land but also their spatial pattern, that can affect the inundation of newly-

developed urban land areas. The height above the nearest drainage (HAND) parameter represents the relative height of each pixel above the elevation of its nearest downstream drainage pixel. As discussed by Nobre et al. (2011)[34], HAND is a good indicator of hydrology-relevant topography such as floodplains. In our study, the HAND data from MERIT Hydro was used to represent the distance of urban land to rivers[35]. These data show that in most of the urban agglomerations (BTH, CP, CSP, YRD, and TCC urban agglomerations), the proportion of urban land with very low HAND (<1 m) is higher under SSP5-8.5 than that in the historical period (Supplementary Fig. 14), which means that the newly-developed urban land is closer to the rivers. This is because most of the newly-developed urban land has grown outwards from the original urban land (i.e., edge-expansion patterns), as a result of the neighborhood effect[26]. In other words, new developments are more likely to occur near places that are already built up. The newly-developed urban land will be closer to the rivers than the original urban land because the latter is already located near the river, as illustrated by urban agglomeration B in Fig. 4a, and by Zhengzhou (Fig. 4d) and Xi'an (Fig. 4e). Consequently, in these urban agglomerations, the proportion of newly-developed urban land distributed in areas inundated by historical 100-year floods is higher than that of the original urban land (Supplementary Table 11). This will lead to the newly-developed urban land being more easily inundated than the original urban land (i.e., the urban agglomeration B in Fig. 4a).

As we can see from Fig. 5, on average, the inundated extent (i.e., areas inundated at least once in 30 years) of newly-developed urban land will be about 10% more than that of the original urban land. This is the other reason why urban land expansion plays a relatively important role in the increase of inundated urban land areas in northern urban agglomerations (i.e., BTH, CP, and CSP urban agglomerations). The YRD urban agglomeration is an exception because unlike the other four urban agglomerations (BTH, CP, CSP, and TCC urban agglomerations), the terrain of the YRD urban agglomeration is relatively flat (Supplementary Fig. 1) and the 100-year floodplains are largest (Supplementary Fig. 24), and thus it is insensitive to changes in HAND. This is also reflected by Fig. 2, in which the inundated proportion of urban land is not larger than the inundated proportion of total land in the YRD urban agglomeration.

We also note that, unlike other urban agglomerations, the proportion of urban land with very low HAND (<1 m) is lower
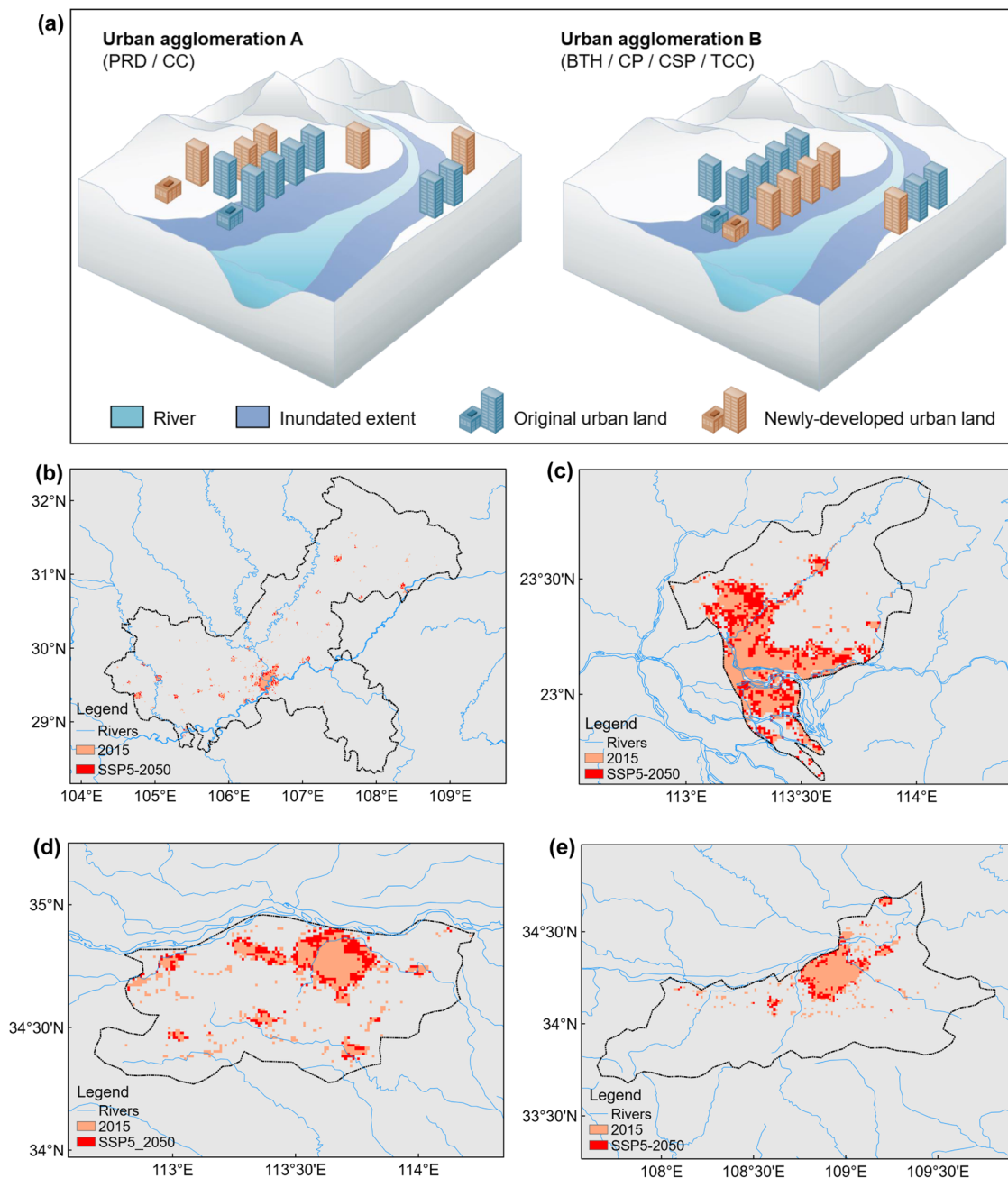
Fig. 4 The spatial distributions of original urban land in the historical period and newly-developed urban land in the future. a The expansion of urban land in two typical urban agglomerations. The urban agglomeration A refers to the urban agglomerations where the historical urban land is closer to the river, while the urban agglomeration B refers to the urban agglomerations where the newly-developed urban land is closer to the river. **b–e** The urban land expansion of Chongqing (**b**), Guangzhou (**c**), Zhengzhou (**d**), and Xi'an (**e**), which are the core cities of the CC, PRD, CP, and CSP urban agglomerations, respectively.

under SSP5-8.5 than that in the historical period in the CC and PRD urban agglomerations (Supplementary Fig. 14). The CC urban agglomeration (e.g., Chongqing) is mountainous, and the PRD urban agglomeration (e.g., Guangzhou) has a high proportion of urban land in the historical period (Supplementary Fig. 1), which means that the land along the rivers has already been developed in the historical period (Fig. 4b, c). In these urban agglomerations, there is not much urban land available. Eventually, the urban land will expand to higher terrain located far away from rivers (i.e., urban agglomeration A in Fig. 4a). This explains why, in these urban agglomerations, the newly-developed urban land is not more easily inundated than the

original urban land (Fig. 5). The same reasoning also applies under SSP3-7.0 (Supplementary Figs. 13 and 15). We suppose that future urban land expansion should avoid flood risk zones as much as possible, and cannot expand indefinitely.

Discussion
Our analyses show that against a background of climate change and urban land expansion, the flood risk (i.e., inundated urban land areas) in China's seven major urban agglomerations is expected to face a 4 to 19 times increase, with southern China facing the greatest increase. It should be noted that there is inevitable uncertainty in projected flood risk. The potential
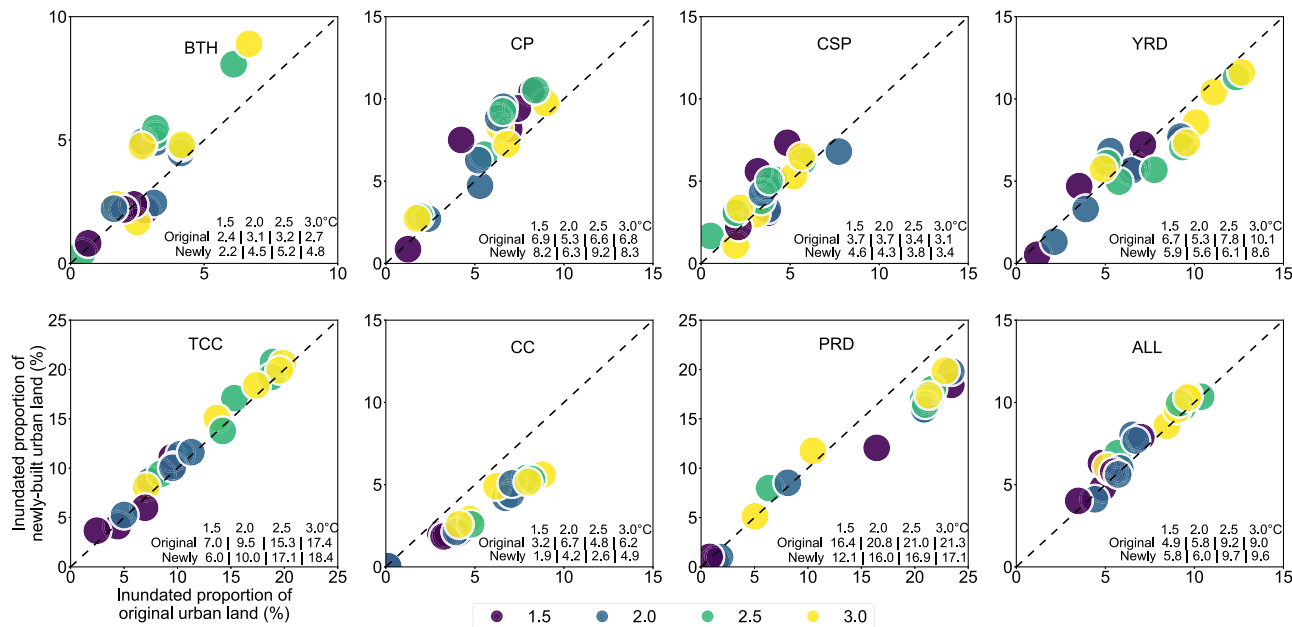
Fig. 5 The inundated urban land extent under SSP5-8.5. The x-axis represents the original 30-year inundated urban land extent as a proportion of the total original urban land area, and the y-axis represents the 30-year inundated newly-developed urban land extent as a proportion of the total newly-developed urban land area. The color of the dots represents the warming level. Each color has five dots, representing five GCMs. The values in the lower right represent the median inundated proportion based on the five GCMs. Note that dots plotting above the 1:1 line show that newly-developed urban land is more likely to be inundated.

sources of uncertainty include the climate forcing, hydrological models, flood frequency analysis, and urban land dataset, among others. The performance of the five GCMs provided by ISIMIP3b in flood simulation and the uncertainty pertaining to the GCMs has been evaluated in Supplementary Note 3. Although the uncertainty pertaining to the GCMs is large, the percentage of the GCMs that agree on the positive sign of the projected change of the inundated urban land areas is high in most of the urban agglomerations (Supplementary Table 5). If only the GCMs that agree on the positive sign of the projected change are considered, the relative rise of multi-model median inundated urban land areas of each urban agglomeration is similar to that consider all GCMs (Supplementary Table 6). Besides, the relative rise of multi-model mean and multi-model median inundated urban land areas is also similar (Supplementary Table 7). Zhou et al.[36] have found that flood simulation results are not sensitive to the fitting distribution when fitting with the river water storage. Here, we also used the three-parameter Weibull distribution to extract floods, and show that the urban land area exposed to floods is projected to rise by 1 to 22 times under the background of urban expansion and climate change (Supplementary Table 8); this is close to the results based on the Gumbel distribution. The uncertainty pertaining to the urban land dataset could be further evaluated when more high-resolution urban land dataset becomes available.

Climate change is the main factor leading to projected increases in inundated urban land areas in China's urban agglomerations. However, in some agglomerations (e.g., BTH urban agglomeration), although the climate change plays a more important role if the warming level is higher than 2 °C, the urban land expansion plays a more important role if the warming level is lower than 2 °C. This highlights the necessity of long-term simulation, which can help policy-makers develop long-term flood prevention strategies. The flood risk of urban land is projected to rise in the future, with particularly sharp rises after 2 °C warming in some urban agglomerations (e.g., YRD and TCC

urban agglomerations in Fig. 1a). Therefore, for disaster prevention and mitigation, it is essential to restrict warming to below 2 °C, or even below 1.5 °C.

Existing research has revealed that the edge-expansion type dominated the growth of urban land in floodplains in China[37]. Our results further reveal that changes in the area and distribution of urban land will increase the inundated urban land areas. The edge-expansion pattern will make part of the newly-developed urban land areas closer to the rivers, and thus newly-developed urban land will be inundated more easily than historical urban land. This finding is applicable not only to China, but also to other regions of the world, especially for countries that are currently undergoing rapid urbanization. This finding also calls for new projections of future flood risks and potential losses which consider urban land expansion in the future, as the flood losses may be underestimated in existing research.

The 100-year flood protection levels performed well in the historical period and were able to reduce inundated urban land areas by over 90% (Supplementary Table 12). As the extent of inundated urban land faces a pronounced increase, the 100-year flood protection level will be unable to meet the flood control demand in the future. The Chinese government is already aware of the urgency to take effective adaptation strategies to minimize the flood losses, and the latest version of China's national flood control standards points out that cities with populations exceeding 1.5 million and a GDP per capita index (i.e., the ratio of the city's GDP per capita to national GDP per capita) greater than 2 should have a 200-year flood protection level or higher (standard no. GB 50201-2014)[37]. However, increased flood protection levels may need large investment, and the residual flood damage could be still large under an adaptation strategy based on feasible adaptation costs[38]. Therefore, to minimize the flood risk and losses, more efforts need to be made to integrate hazard reduction (i.e., controlling global warming), exposure reduction (i.e., reasonable urban planning), and vulnerability reduction (i.e., strengthened flood protection levels).

This research has some limitations. Firstly, human activities such as reservoir construction, water withdrawal and drainage networks within cities have not been considered here, and therefore the projected inundated urban land may be over-estimated. We should also note that the projected urban land expansion data is based on Future Land-Use Simulation model, which does not consider flood risk for urban expansion. As shown in Fig. 1b, c, even if we assumed that climate will not change in the future (i.e., only urban land expansion is considered), the inundation areas in the future (i.e., the blue bars in Fig. 1b, c) are also larger than those in the historical period (i.e., the black bars in Fig. 1b, c), which means that some newly-developed urban land will lie in areas inundated by historical 100-year floods. Therefore, the projected inundated urban land areas may be slightly overestimated. Nowadays, there are some models that can simulate urban land change by considering flood risk. Under the framework of the shared socioeconomic pathways, future research can use these models to project the urban land expansion by considering flood risk[39,40]. Besides, the changes in geology and hydrology due to urbanization were not considered, but previous research show that urbanization can enhance runoff generation and hence flood peaks, although these effects are most evident in small catchments[41,42]. Lastly, in addition to the seven urban agglomerations, there are other urban agglomerations in China that may face similar risks, and further investigation is needed in future research.

Methods

Forcing data. We used five of the latest bias-corrected forcings from five global circulation models (GCMs) provided by phase 3b of the Inter-Sectoral Impact Model Intercomparison Project (ISIMIP3b) as forcing data[43]. The bias-adjustment corrects the simulated data towards corrected ERA5 observational data (i.e., W5E5). Compared with other bias adjustment method, the ISI-MIP3 bias adjustment method allow for a more robust bias adjustment of extreme values, preserving trends more accurately across quantiles[43]. The contributing models were GFDL-ESM4, IPSL-CM6A-LA, MPI-ESM1-2-HR, MRI-ESM2-0, and UKESM1-0-LL. All the GCMs cover the period from 1850 to 2100, with an initial spatial resolution of 0.5°, and the data were interpolated to 0.25° resolution using the bilinear interpolation method. The five models are good representatives of the whole CMIP6 ensemble, and the bias-corrected forcing preserves the simulated warming signal[44]. Daily maximum temperature, minimum temperature, precipitation, and wind speed data were selected, and the historical, SSP1-2.6, SSP3-7.0, and SSP5-8.5 scenarios were considered because when our study started, only these three scenarios were available. SSP1-2.6 is the "sustainability" SSP1 socio-economic family, with a warming level of 2 °C. SSP3-7.0 is a medium-high reference scenario within the "regional rivalry" socio-economic family. SSP5-8.5 is a high reference scenario in a high fossil-fuel development world, with the strongest warming[45]. We have also verified the applicability of bias-corrected forcing data in China (See Supplementary Note 3).

We present changes in flood risk between the reference period (1985–2014) and 30-year windows centered on the years when global average temperatures are 1.5, 2, 2.5, and 3 °C above the preindustrial temperature, as obtained from ISIMIP3b temperature thresholds and time slices (Supplementary Table 3). Under SSP1-2.6, only UKESM1-0-LL can reach warming levels of 2 °C and 2.5 °C, so we only consider a 1.5 °C warmer climate under this scenario. Even with the climate warming limited to 1.5 °C, only four of the GCMs can reach it.

To verify the applicability of the model framework established by this study in China (See Supplementary Notes 1 and 2), the China Meteorological Forcing Dataset (CMFD) was also selected as the historical forcing data[46,47]. This dataset combines historical observations, remote sensing data, and meteorological reanalysis data, and has been shown to have high accuracy[48]. The data were interpolated from 0.1° to 0.25° resolution using bilinear interpolation. Following a published approach[32], because the flood depth and inundation areas calculated from the GCMs may be unreasonable due to inevitable precipitation biases, the flood depth generated by CMFD was also used to establish flood depth–recurrence frequency relationships. This allowed transformation of the GCM-simulated flood recurrence to the flood depth generated by CMFD.

Flood simulation. Daily runoff at the 0.25° scale was simulated by the VIC model in China, which is a grid-based, large-scale, distributed hydrological model developed by the University of Washington[49]. It has a strong physical basis and considers sub-grid-scale soil water storage capacity and vegetation spatial distribution. VIC has been successfully applied to runoff simulations of the world's major rivers[50–52]. The input data include daily maximum temperature, minimum temperature, precipitation, and wind speed from ISIMIP3b and CMFD. The soil and vegetation parameters required for model operation are consistent with previous studies and have been carefully calibrated in China[53].

The daily runoff data generated by the VIC model were further used as input data to drive the global hydrodynamic model CaMa-Flood v3.6.2[54], to generate daily river discharge, river water storage, flood depth, and flood inundation areas with a spatial resolution of 0.25°. The river width data used here are GWD-LR[55], and the river depth was carefully calibrated by trial and error. The inundation depths computed at 0.25° were downscaled onto an 18-arcsec (approximately 500 m at the equator) high-resolution digital elevation model (DEM) by determining whether the elevation of the DEM pixels was lower than the modeled water level[9]. Because CaMa-Flood incorporates the same high-resolution sub-grid topography, the water volume before and after downscaling is consistent. This downscaling method is now widely used in flood risk research[32,38,56]. The same downscaling method has also been used in calculating flood damage in urban land in previous research[8,24]. Compared with the general routing model, CaMa-Flood is characterized by introducing the concept of the floodplain through sub-grid parameterization, which can simulate the water storage, water depth, and inundation of floodplains[54]. CaMa-Flood has been widely used to generate global and regional flood hazard maps, and the results show that it has strong flood inundation simulation capabilities[9,32,57].

To the best of our knowledge, there are only two sets of flood protection levels available for China[58,59]. The data from Wang et al.[59] represent the flood protection levels of the year 2015, while the historical period in this study is from 1985 to 2014. Besides, the data from Wang et al.[59] focus on the county-level flood protection levels, while the resolution of the simulated flood inundation maps in this study is nearly 500 m. The data from Scussolini et al.[58] show that the flood protection levels for the majority of provinces in China, including Beijing, has a return period of 20 years, which is not consistent with the large-scale reservoir construction and the gradual completion of flood protection facilities in China over the past decades[60]. Previous studies set the flood protection levels as a return period of 100 years for countries such as Egypt, where large dam systems were built[9]. Thus, here we only consider floods exceeding the 100-year return period. The magnitude of 100-year floods in each 0.25° pixel is calculated by fitting the time series of historical 30-year

annual maximum daily river water storage to the Gumbel probability distribution function[61]. The applicability of the Gumbel probability distribution in flood extraction has been validated in the previous studies[10,32,62].

The results of previous studies indicate that the Gumbel distribution is not suitable for extreme arid areas[32], and the flood risk in arid areas is relatively small. Therefore, areas with 30-year average runoff (simulated by CMFD forcing data) less than 0.02 mm/day are not considered here. For validation of the above model cascade please see Supplementary Notes 1 and 2.

Calculation of flood risk. The future urban land expansion data were obtained from Chen et al.[26], and were interpolated from the original 1-km to 18-arcsec resolution (about 500 m at the equator) by nearest neighbor interpolation, to match the resolution of the inundation map. This dataset provides the world's first 1-km resolution projections of global urban land expansion under the framework of the shared socioeconomic pathways. Firstly, a regression model which was built through historical urban land, population, urbanization rate and gross domestic product, was used to project the future urban land demand for each scenario. Then, the spatial distribution of urban land expansion was simulated by using the Future Land-Use Simulation model[63]. The Future Land-Use Simulation model was developed within the framework of cellular automata, which assumes that the probability of a non-urban grid being transformed into an urban grid is a product of the urban development potential, the neighborhood effect, the development constraint and the adjustment factor. The artificial neural networks were used to estimate the urban development potential, taking into account a number of spatial driving factors (e.g., population, gross domestic product, distance to city center, distance to road network). The neighborhood effect factor is calculated as the proportion of existing urban land area in a neighborhood consisting of 5×5 grids[26]. The data were generated by considering the spatial expansion of urban land, and thus can be used to study the effect of urban land expansion on flood risk. For the historical period, the reference year for urban land area is 2015. For future periods, because we only have urban land data for each decade, we selected data closest to the years in which the global average temperatures are 1.5, 2, 2.5, and 3 °C above the preindustrial temperature. Our study covers the following variables: the urban agglomeration areas (A), urban land areas (Au), non-urban land areas (Ar), inundated areas of the urban agglomeration (I), inundated urban land areas (Iu), inundated non-urban land areas (Ir), inundated proportion of the total land (P), inundated proportion of the urban land (Pu) and inundated proportion of the non-urban land (Pr). These variables are related by the following equations:

$$A = A_u + A_r \tag{1}$$

$$I = I_u + I_r \tag{2}$$

$$P = I/A \tag{3}$$

$$P_u = I_u/A_u \tag{4}$$

$$P_r = I_r/A_r \tag{5}$$

To further study the impact of climate change and urban expansion on flood risk, three different assumptions were made. (1) Only social-economic development is considered (represented here by 'SSP'). The flood hazards in the future will be exactly the same as those in the historical period. (2) Only climate change is considered, such that future urban land data remain unchanged from the historical period (represented here by 'RCP'). (3) Both climate change and urban expansion are considered (represented

here by 'SSP-RCP'). Under each assumption, the inundated urban land areas in each urban agglomeration were obtained by overlaying the urban land data on the flood inundation maps.

The relative contributions of future climate change and urban expansion to changes in flood risk were calculated as follows[30]:

$$\sigma_{ssp} = \frac{E_{ssp}}{E_0} - 1 \tag{6}$$

$$\sigma_{rcp} = \frac{E_{rcp}}{E_0} - 1 \tag{7}$$

$$C_{ssp} = \frac{\sigma_{ssp}}{|\sigma_{ssp}| + |\sigma_{rcp}|} \times 100 \tag{8}$$

$$C_{rcp} = \frac{\sigma_{rcp}}{|\sigma_{ssp}| + |\sigma_{rcp}|} \times 100 \tag{9}$$

Here, E_0, E_{ssp} and E_{rcp} represent the urban land that will be inundated in the historical period, if only socio-economic conditions are changed, and if only climate is changed in the future, respectively. C_{rcp} and C_{ssp} represent the contributions of climate change and urban expansion, respectively. The greater the absolute value, the higher the contribution, and a negative value implies a negative effect.

References

1. The human cost of weather-related disasters 1995-2015. (UNISDR & CRED, 2015). https://www.unisdr.org/files/.
2. Jiang, T. et al. Each 0.5 °C of warming increases annual flood losses in China by more than US$60 billion. *Bull. Am. Meteorol. Soc.* **101**, E1464–E1474 (2020).
3. Huntington, T. G. Evidence for intensification of the global water cycle: review and synthesis. *J. Hydrol.* **319**, 83–95 (2006).
4. Climate Change 2021: The Physical Science Basis. (IPCC, 2021). https://www.ipcc.ch/report/.
5. Wu, H., Huang, M., Tang, Q., Kirschbaum, D. B. & Ward, P. Hydrometeorological hazards: monitoring, forecasting, risk assessment, and socioeconomic responses. *Adv. Meteorol.* **2016**, 1–3 (2016).
6. Mao, Y. et al. Flood inundation generation mechanisms and their changes in 1953–2004 in global major river basins. *J. Geophys. Res.: Atmos.* **124**, 11672–11692 (2019).
7. Alfieri, L. et al. Global projections of river flood risk in a warmer world. *Earth's Future* **5**, 171–182 (2017).
8. Ward, P. J. et al. A global framework for future costs and benefits of river-flood protection in urban areas. *Nat. Clim. Change* **7**, 642–646 (2017).
9. Dottori, F. et al. Increased human and economic losses from river flooding with anthropogenic warming. *Nat. Clim. Change* **8**, 781–786 (2018).
10. Boulange, J., Hanasaki, N., Yamazaki, D. & Pokhrel, Y. Role of dams in reducing global flood exposure under climate change. *Nat. Commun.* **12**, 417 (2021).

11. Eyring, V. et al. Overview of the Coupled Model Intercomparison Project Phase 6 (CMIP6) experimental design and organization. *Geosci. Model Dev.* **9**, 1937–1958 (2016).

12. Kundzewicz, Z. W. et al. Flood risk and its reduction in China. *Adv. Water Resour.* **130**, 37–45 (2019).

13. Xin, X., Wu, T., Zhang, J., Yao, J. & Fang, Y. Comparison of CMIP6 and CMIP5 simulations of precipitation in China and the East Asian summer monsoon. *Int. J. Climatol.* **40**, 6423–6440 (2020).

14. Zhu, H. et al. Does CMIP6 inspire more confidence in simulating climate extremes over China. *Adv. Atmos. Sci.* **37**, 1119–1132 (2020).

15. Hirabayashi, Y., Tanoue, M., Sasaki, O., Zhou, X. & Yamazaki, D. Global exposure to flooding from the new CMIP6 climate model projections. *Sci. Rep.* **11**, 3740 (2021).

16. Jongman, B., Ward, P. J. & Aerts, J. C. J. H. Global exposure to river and coastal flooding: Long term trends and changes. *Glob. Environ. Change* **22**, 823–835 (2012).

17. Tanoue, M., Hirabayashi, Y. & Ikeuchi, H. Global-scale river flood vulnerability in the last 50 years. *Sci. Rep.* **6**, 36021 (2016).

18. Sauer, I. J. et al. Climate signals in river flood damages emerge under sound regional disaggregation. *Nat. Commun.* **12**, 2128 (2021).

19. Tellman, B. et al. Satellite imaging reveals increased proportion of population exposed to floods. *Nature* **596**, 80–86 (2021).

20. Du, S., He, C., Huang, Q. & Shi, P. How did the urban land in floodplains distribute and expand in China during 1992–2015? *Environ. Res. Lett.* **13**, https://doi.org/10.1088/1748-9326/aaac07 (2018).

21. Chen, W. et al. Countermeasures for rainstorm and flood prevention in high-density cities—the "7·20" heavy rain revelation in Zhengzhou. *China Water Resour.* **15**, 18–23 (2021).

22. Güneralp, B., Güneralp, İ. & Liu, Y. Changing global patterns of urban exposure to flood and drought hazards. *Glob. Environ. Change* **31**, 217–225 (2015).

23. Mustafa, A., Bruwier, M., Archambeau, P. & Erpicum, S. Effects of spatial planning on future flood risks in urban environments. *J. Environ. Manag.* **225**, 193–204 (2018).

24. Winsemius, H. C. et al. Global drivers of future river flood risk. *Nat. Clim. Change* **6**, 381–385 (2015).

25. Muis, S., Güneralp, B., Jongman, B., Aerts, J. C. J. H. & Ward, P. J. Flood risk and adaptation strategies under climate change and urban expansion: A probabilistic analysis using global data. *Sci. Total Environ.* **538**, 445–457 (2015).

26. Chen, G. et al. Global projections of future urban land expansion under shared socioeconomic pathways. *Nat. Commun.* **11**, 537 (2020).

27. Alfieri, L., Feyen, L., Dottori, F. & Bianchi, A. Ensemble flood risk assessment in Europe under high end climate scenarios. *Glob. Environ. Change* **35**, 199–212 (2015).

28. Sampson, C. C. et al. A high-resolution global flood hazard model. *Water Resour. Res.* **51**, 7358–7381 (2015).

29. Wang, J. et al. Modeling daily floods in the lancang-mekong river basin using an improved hydrological-hydrodynamic model. *Water Resour. Res.* **57**, e2021WR029734 (2021).

30. Vousdoukas, M. I. et al. Climatic and socioeconomic controls of future coastal flood risk in Europe. *Nat. Clim. Change* **8**, 776–780 (2018).

31. Arnell, N. W. & Gosling, S. N. The impacts of climate change on river flood risk at the global scale. *Clim. Change* **134**, 387–401 (2014).

32. Hirabayashi, Y. et al. Global flood risk under climate change. *Nat. Clim. Change* **3**, 816–821 (2013).

33. Asadieh, B. & Krakauer, N. Y. Global change in streamflow extremes under climate change over the 21st century. *Hydrol. Earth Syst. Sci.* **21**, 5863–5874 (2017).

34. Nobre, A. D. et al. Height above the nearest drainage—a hydrologically relevant new terrain model. *J. Hydrol.* **404**, 13–29 (2011).

35. Yamazaki, D. et al. MERIT hydro: a high-resolution global hydrography map based on latest topography dataset. *Water Resour. Res.* **55**, 5053–5073 (2019).

36. Zhou, X., Ma, W., Echizenya, W. & Yamazaki, D. The uncertainty of flood frequency analyses in hydrodynamic model simulations. *Natural Hazards. Earth Syst. Sci.* **21**, 1071–1085 (2021).

37. Han, Y. et al. The growth mode of built-up land in floodplains and its impacts on flood vulnerability. *Sci. Total Environ.* **700**, 134462 (2020).

38. Tanoue, M., Taguchi, R., Alifu, H. & Hirabayashi, Y. Residual flood damage under intensive adaptation. *Nat. Clim. Change* **11**, 823–826 (2021).

39. Filatova, T., Voinov, A. & van der Veen, A. Land market mechanisms for preservation of space for coastal ecosystems: an agent-based analysis. *Environ. Modelling. Softw.* **26**, 179–190 (2011).

40. de Koning, K., Filatova, T., Need, A. & Bin, O. Avoiding or mitigating flooding: bottom-up drivers of urban resilience to climate change in the USA. *Glob. Environ. Change* **59**, 101981 (2019).

41. Gori, A., Blessing, R., Juan, A., Brody, S. & Bedient, P. Characterizing urbanization impacts on floodplain through integrated land use, hydrologic, and hydraulic modeling. *J. Hydrol.* **568**, 82–95 (2019).

42. Merz, B. et al. Causes, impacts and patterns of disastrous river floods. *Nat. Rev. Earth. Environ.* **2**, 592–609 (2021).

43. Lange, S. Trend-preserving bias adjustment and statistical downscaling with ISIMIP3BASD (v1.0). *Geosci. Model Dev.* **12**, 3055–3070 (2019).

44. Jägermeyr, J. et al. Climate impacts on global agriculture emerge earlier in new generation of climate and crop models. *Nat. Food* **2**, 873–885 (2021).

45. O'Neill, B. C. et al. The Scenario Model Intercomparison Project (ScenarioMIP) for CMIP6. *Geosci. Model Dev.* **9**, 3461–3482 (2016).

46. Yang, K., He, J., Tang, W., Qin, J. & Cheng, C. C. K. On downward shortwave and longwave radiations over high altitude regions: Observation and modeling in the Tibetan Plateau. *Agric. Forest Meteorol.* **150**, 38–46 (2010).

47. He, J. et al. The first high-resolution meteorological forcing dataset for land process studies over China. *Sci. Data* **7**, 25 (2020).

48. Yang, F. et al. Evaluation of multiple forcing data sets for precipitation and shortwave radiation over major land areas of China. *Hydrol. Earth Syst. Sci.* **21**, 5805–5821 (2017).

49. Liang, X. & Lettenmaier, D. P. A simple hydrologically based model of land surface water and energy fluxes for general circulation models. *J. Geophys. Res.: Atmo.* **99**, 14415–14428 (1994).

50. Nijssen, B., O'Donnell, G. M., Hamlet, A. F. & Lettenmaier, D. P. Hydrologic sensitivity of global rivers to climate change. *Clim. Change* **50**, 143–175 (2001).

51. Raje, D., Priya, P. & Krishnan, R. Macroscale hydrological modelling approach for study of large scale hydrologic impacts under climate change in Indian river basins. *Hydrol. Processes* **28**, 1874–1889 (2014).

52. Naz, B. S. et al. Effects of climate change on streamflow extremes and implications for reservoir inflow in the United States. *J. Hydrol.* **556**, 359–370 (2018).

53. Zhang, X.-J., Tang, Q., Pan, M. & Tang, Y. A long-term land surface hydrologic fluxes and states dataset for China. *J. Hydrometeorol.* **15**, 2067–2084 (2014).

54. Yamazaki, D., Kanae, S., Kim, H. & Oki, T. A physically based description of floodplain inundation dynamics in a global river routing model. *Water Resour. Res.* **47**, https://doi.org/10.1029/2010wr009726 (2011).

55. Yamazaki, D. et al. Development of the Global Width Database for large rivers. *Water Resour. Res.* **50**, 3467–3480 (2014).

56. Pappenberger, F., Dutra, E., Wetterhall, F. & Cloke, H. L. Deriving global flood hazard maps of fluvial floods through a physical model cascade. *Hydrol. Earth Syst. Sci.* **16**, 4143–4156 (2012).

57. Lu, X., Zhuang, Q., Liu, Y., Zhou, Y. & Aghakouchak, A. A large-scale methane model by incorporating the surface water transport. *J. Geophys. Res.: Biogeosci.* **121**, 1657–1674 (2016).

58. Scussolini, P., Aerts, J. C. J. H., Jongman, B. & Bouwer, L. M. FLOPROS an evolving global database of flood protection standards. *Natural Hazards Earth Syst. Sci.* **16**, 1049–1061 (2016).

59. Wang, D., Scussolini, P. & Du, S. Assessing Chinese flood protection and its social divergence. *Natural Hazards Earth Syst. Sci.* **21**, 743–755 (2021).

60. Du, S. et al. Brief communication: rethinking the 1998 China floods to prepare for a nonstationary future. *Natural Hazards Earth Syst. Sci.* **19**, 715–719 (2019).

61. Hosking, J. R. M. L-moments: analysis and estimation of distributions using linear combinations of order statistics. *J. Royal Statistical Soc. Ser. B (Methodol.)* **52**, 105–124 (1990).

62. Ward, P. J. et al. Assessing flood risk at the global scale: model setup, results, and sensitivity. *Environ. Res. Lett.* **8**, 044019 (2013).

63. Liu, X. et al. A future land use simulation model (FLUS) for simulating multiple land use scenarios by coupling human and natural effects. *Landscape Urban Planning* **168**, 94–116 (2017).

Acknowledgements

Author contributions

H.L. designed the research. R.J. conducted the experiments and analysis. K.Y., D.Y., M.P., and Y.Y. provided the materials. R.J. wrote the manuscript. H.L., D.C., K.Y., and D.Y. revised the manuscript. J.Z., M.P, W.L., N.X., D.G., and F.T. helped interpret the results. All authors contributed to the discussion of the results.

Competing interests

The authors declare no competing interests.

Additional information

Supplementary information The online version contains supplementary material available at https://doi.org/10.1038/s43247-023-01049-0.

Correspondence and requests for materials should be addressed to Hui Lu.

Peer review information *Communications Earth & Environment* thanks the anonymous reviewers for their contribution to the peer review of this work. Primary Handling Editor: Joe Aslin. A peer review file is available.

Reprints and permission information is available at http://www.nature.com/reprints

Publisher's note Springer Nature remains neutral with regard to jurisdictional claims in published maps and institutional affiliations.